IAI Journals.ASM.org

Interactions between Polymorphonuclear Leukocytes and *Pseudomonas aeruginosa* Biofilms on Silicone Implants *In Vivo*

Maria van Gennip,[a] Louise Dahl Christensen,[a] Morten Alhede,[a,c] Klaus Qvortrup,[b] Peter Østrup Jensen,[c] Niels Høiby,[a,c] Michael Givskov,[a,d] and Thomas Bjarnsholt[a,c]

Department of International Health, Immunology and Microbiology, University of Copenhagen, Copenhagen, Denmark[a]; Department of Biomedical Sciences, University of Copenhagen, Copenhagen, Denmark[b]; Department of Clinical Microbiology, Rigshospitalet, Copenhagen, Denmark[c]; and Singapore Centre on Environmental Life Sciences Engineering, Nanyang Technological University, Singapore, Singapore[d]

Chronic infections with *Pseudomonas aeruginosa* persist because the bacterium forms biofilms that are tolerant to antibiotic treatment and the host immune response. Scanning electron microscopy and confocal laser scanning microscopy were used to visualize biofilm development *in vivo* following intraperitoneal inoculation of mice with bacteria growing on hollow silicone tubes, as well as to examine the interaction between these bacteria and the host innate immune response. Wild-type *P. aeruginosa* developed biofilms within 1 day that trapped and caused visible cavities in polymorphonuclear leukocytes (PMNs). In contrast, the number of cells of a *P. aeruginosa rhlA* mutant that cannot produce rhamnolipids was significantly reduced on the implants by day 1, and the bacteria were actively phagocytosed by infiltrating PMNs. In addition, we identified extracellular wire-like structures around the bacteria and PMNs, which we found to consist of DNA and other polymers. Here we present a novel method to study a pathogen-host interaction in detail. The data presented provide the first direct, high-resolution visualization of the failure of PMNs to protect against bacterial biofilms.

Understanding the biofilm phenotype of chronic infections has helped to explain why antibiotic concentrations recommended by clinical microbiology laboratories often fail in treating these infections (15). Bacteria in biofilms are aggregated and often sessile, and they differ from free-floating cells by their slow growth and tolerance to antibiotics. To elucidate mechanisms involved in the biofilm phenotype, researchers have extensively investigated the phenomenon by using the opportunistic Gram-negative pathogen *Pseudomonas aeruginosa* both *in vitro* and *in vivo*. *P. aeruginosa* is frequently isolated from foreign body infections (4) and chronic wounds (21, 25) and is the primary bacterium isolated from the lungs of cystic fibrosis (CF) patients with chronic infections, where *P. aeruginosa* resides as a biofilm (34).

Poor antibiotic efficacy is not the only problem in the fight against biofilms. Chronic infections develop because the innate immune response is ineffective at clearing biofilm infections, irrespective of the location of the biofilm in the host (8, 25). Within the innate immune response, phagocytic cells such as macrophages and polymorphonuclear leukocytes (PMNs) act as the first line of host defense (33). PMNs are recruited from the blood in response to a series of inflammatory signals (reviewed in reference 10). After arrival at the site of infection, PMNs start to phagocytose invading bacteria and contribute to the development of inflammation. Resolution of inflammation involves PMN apoptosis and engulfment by macrophages, a process that leads to division of granule content and fragmentation of the PMNs, which serve to limit the release of toxic molecules such as elastase, oxidants, and nuclear DNA that would otherwise damage host tissue (16). In normal tissue, such as in the lung, the massive PMN recruitment that occurs in response to acute infection can usually be resolved successfully, and the tissue will regenerate once the infection is cleared (16).

Foreign body-related infections involve primarily Gram-positive bacteria such as staphylococci (reviewed in reference 37). The bacterial colonization most likely occurs following contamination of the medical device from the patient's skin or mucous membranes or from the hands of the clinical staff during implantation (37). Although they are less common, foreign body-related infections with Gram-negative bacteria tend to be more severe (19). Gram-negative bacteria such as *P. aeruginosa* have been cultivated from urines of trauma patients with catheter-associated bacteriuria (18) and from peritoneal catheters in peritoneal dialysis patients (17), and in these cases the bacteria frequently form biofilms. Biofilm formation on foreign bodies proceeds by initial adhesion and attachment followed by proliferation and biofilm formation (37). Biofilms on the surfaces of infected foreign bodies persist despite host defense mechanisms. Antibiotics also frequently fail to eradicate the infection, leaving removal of the implant as the only option for resolving the infection (reviewed in reference 37).

The immune response in the peritoneal cavity involves PMNs (reviewed in references 13, 19, and 39) and is very effective against bacterial infections that do not involve a medical device. After initial infections, bacteria are removed via the lymphatics and pass into the systemic circulation, where the reticuloendothelial system clears them from the blood or they are filtered out at retrosternal lymph nodes (39). The peritoneal cellular defenses are subsequently activated, leading to clearance of bacteria from the peritoneum (39). In contrast, introduction of a foreign body into the

Received 30 November 2011 **Returned for modification** 26 January 2012
Accepted 4 May 2012
Published ahead of print 14 May 2012
Editor: B. A. McCormick
Address correspondence to Thomas Bjarnsholt, tbjarnsholt@sund.ku.dk.
Supplemental material for this article may be found at http://iai.asm.org/.

doi:10.1128/IAI.06215-11

peritoneal cavity followed by a bacterial challenge results in rapid colonization of the implant and the establishment of chronic infection (39). The implant also becomes coated with plasma and connective tissue proteins such as fibronectin, fibrinogen, vitronectin, thrombospondin, laminin, collagen, and von Willebrand factor (37).

In 1991, Buret et al. (13) described a biofilm model in rabbits for investigating the evolution and organization of a *P. aeruginosa* biofilm on a silastic subdermal implant by use of light microscopy and transmission electron microscopy (TEM). In 2007, a new model for studying *in vivo* biofilms was published by Christensen et al. (14). This model involves the introduction of a flat silicone implant into the peritoneal cavity of mice precolonized with *P. aeruginosa* and was designed to test the efficacy of quorum sensing inhibitors (QSIs) in the treatment of biofilm infections. Using the model of Christensen et al. (14) in parallel with a pulmonary *P. aeruginosa* infection model, we showed that disabling the QS systems with QSIs or by mutation increased the sensitivity of the biofilm to the innate immune response and enabled PMNs to clear the biofilm infection (6, 7, 36).

In the interplay between biofilms and PMNs, rhamnolipids are a particularly important virulence factor. Jensen et al. (23) showed that rhamnolipids produced by *P. aeruginosa* cause PMNs to undergo necrotic death, and Alhede et al. (1) showed that *P. aeruginosa* responds to the presence of PMNs by upregulating the synthesis of rhamnolipids. Using a pulmonary infection model and the model of Christensen et al., it was shown that an *rhlA* mutant was cleared from the lung more quickly than wild-type (WT) *P. aeruginosa*, suggesting that rhamnolipids mediate protection against PMNs (36).

However, the direct interplay and the failure of PMNs to phagocytose *P. aeruginosa* in a biofilm have never been observed directly *in vivo*. Therefore, the model of Christensen et al. (14) was modified by use of hollow tubes instead of flat implants to allow visualization of this phenomenon. The hollow tubes allow for visualization of the biofilm and its interaction with the host cellular response by use of both scanning electron microscopy (SEM) and confocal laser scanning microscopy (CLSM). In this study, it was used to visualize the protective role of rhamnolipids against PMNs in the infection process by examination of implants from mice inoculated with a *P. aeruginosa rhlA* mutant or WT strain.

MATERIALS AND METHODS

Bacterial strains. All experiments were performed with a WT *P. aeruginosa* PAO1 strain and its isogenic derivatives, obtained from Barbara Iglewski (University of Rochester Medical Center, NY). Construction of the isogenic *rhlA*::*gentamicin* mutant was carried out as described earlier (32). The strains were tagged with a plasmid-based mini-Tn*7* transposon system (pBK-miniTn7-*gfp*3) constitutively expressing a stable green fluorescent protein according to the method of Koch et al. (26).

Growth of bacteria. Bacteria from freezer stocks were plated onto blue agar plates (State Serum Institute, Denmark) and incubated at 37°C overnight. Blue agar plates (containing bromothymol blue) (SSI, Denmark) are selective for Gram-negative bacilli (22). One colony was used to inoculate overnight cultures grown in LB medium at 37°C with shaking.

Animals. Female BALB/c mice were purchased from Taconic M&B A/S (Ry, Denmark) at 8 weeks of age and were maintained on standard mouse chow and water *ad libitum* for 2 weeks before challenge.

The animal studies were carried out in accordance with the *European Convention and Directive for the Protection of Vertebrate Animals used for Experimental and Other Scientific Purposes* (15a) and the Danish law on animal experimentation. All experiments were authorized and approved by the National Animal Ethics Committee, Denmark (The Animal Experiments Inspectorate [http://www.justitsministeriet.dk/dyreforsoeg.html]), and were given the permit number 2010/561-1817.

Foreign body infection model. The foreign body infection model was carried out as previously described (9, 14), but with the following modifications: the silicone tubes (inner diameter, 4.0 mm; outer diameter, 6.0 mm; wall thickness, 1.0 mm) (Pumpeslange 60 Shore A; Ole Dich Instrumentmakers Aps) were cut to a height of 4 mm, and the bacterial pellet from a centrifuged overnight culture was resuspended in 0.9% NaCl to an optical density at 600 nm (OD_{600}) of 0.1.

Mice were anesthetized by subcutaneous (s.c.) injections in the groin area with Hypnorm-midazolam (Roche) (Hypnorm [0.315 mg fentanyl citrate ml^{-1} and 10 mg fluanisone ml^{-1}] plus midazolam [5 mg ml^{-1}] and sterile water [1:1:2]). For postoperative pain, the mice received bupivacaine and Temgesic. Pentobarbital (DAK) (10.0 ml kg^{-1} body weight) was injected intraperitoneally (i.p.) to euthanize the mice at the end of the experiments.

Quantitative bacteriology. After removal from the mice, silicone implants were placed in centrifuge tubes containing 2 ml 0.9% NaCl and kept on ice until the tubes were placed in an ultrasound bath (Bransonic model 2510 bath; Branson Ultrasonic Corporation) for 10 min (5 min of degassing followed by 5 min of sonic treatment). Following the ultrasound treatment, the samples were vortexed, serially diluted, and plated on blue agar plates. The plates were incubated at room temperature for 2 days before determination of CFU.

DNase treatment. To evaluate the "wire-like" structures observed by propidium iodide (PI) staining, we immersed implants from 1 and 2 days postinsertion (dpi) in either 1 ml of phosphate-buffered saline (PBS) containing 125 units Benzonase nuclease (Sigma-Aldrich, GmbH, Germany) or PBS alone.

Preparation for SEM. The silicone implants and pure salmon sperm DNA were fixed in 2% glutaraldehyde in 0.05 M sodium phosphate buffer (pH 7.4). After three rinses in 0.15 M sodium phosphate buffer (pH 7.4), specimens were postfixed in 1% OsO_4 in 0.12 M sodium cacodylate buffer (pH 7.4) for 2 h. Following a rinse in distilled water, the specimens were dehydrated to 100% ethanol according to standard procedures and critical point dried (Balzers CPD 030 instrument) using CO_2. The specimens were subsequently mounted on stubs, using colloidal coal as an adhesive, and sputter coated with gold (Polaron SEM E5000 coating unit). Specimens were examined with a Philips FEG30 scanning electron microscope operated at an accelerating voltage of 2 kV.

Staining procedures for *ex vivo* implants. To visualize PMNs and biofilms, the tubes were cut into eight pieces with a scalpel and stained after removal from the mice. The cut concave tubes were placed in a flow cell with a cover slide on top. Cell viability was assessed using PI (P-4170; Sigma) at 10 μM for visualizing dead cells and extracellular DNA (eDNA) as red fluorescence and with Syto9 (Invitrogen) at 2.5 μM for visualizing live cells as green fluorescence. All observations and image acquisitions were performed using a confocal laser scanning microscope (Leica TCS SP5 [Leica Microsystems, Germany] or LSM 710 [Zeiss, Germany]). Images were obtained with a 63× oil or dry objective or a 100× oil objective. Image scanning was carried out with 488-nm (green) and 543-nm (red) laser lines from an Ar-Kr laser. Imaris software (Bitplane AG) was used to generate images of the biofilm.

Statistics. All statistical analyses were performed with GraphPad Prism, version 5.0 (GraphPad Software, San Diego, CA). The test for normality on the bacteriology results did not confirm a Gaussian distribution for all data sets; therefore, a nonparametric Mann-Whitney test was chosen to compare the medians for the different treatment regimens. *P* values of ≤0.05 were considered significant.

RESULTS

Growth of *P. aeruginosa* on hollow silicone implants. The implants used in the modified model were hollow silicone tubes,

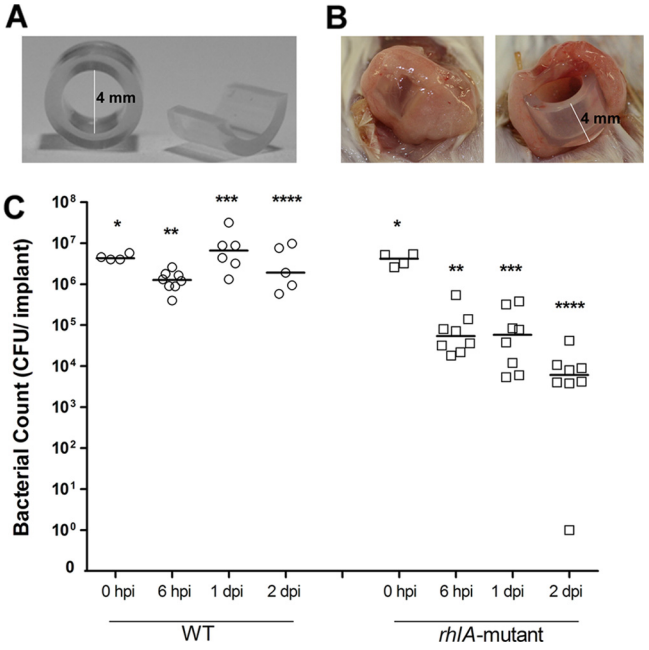

FIG 1 Implant inserted into the mouse peritoneal cavity. (A) Hollow silicone tube used in the mouse model, with an inner diameter of 4 mm. (B) Implants encapsulated in fat tissue at 3 dpi. (C) Bacterial clearance of WT *P. aeruginosa* and the *rhlA* mutant. There was a significant difference in the number of CFU recovered for mice infected with WT *P. aeruginosa* compared to mice infected with the *rhlA* mutant at 6 hpi (**, $P < 0.0003$), 1 dpi (***, $P < 0.002$), and 2 dpi (****, $P < 0.002$). There was no significant difference at 0 hpi (*, $P < 0.66$). Circles and squares represent the numbers of CFU per implant for individual mice; bars represent the medians. The Mann-Whitney U test (analysis of nonparametric data) was used to compare bacterial counts for calculating *P* values in the statistical program GraphPad Prism, version 5.0 (GraphPad Software, Inc., San Diego, CA). *P* values of ≤0.05 were considered significant.

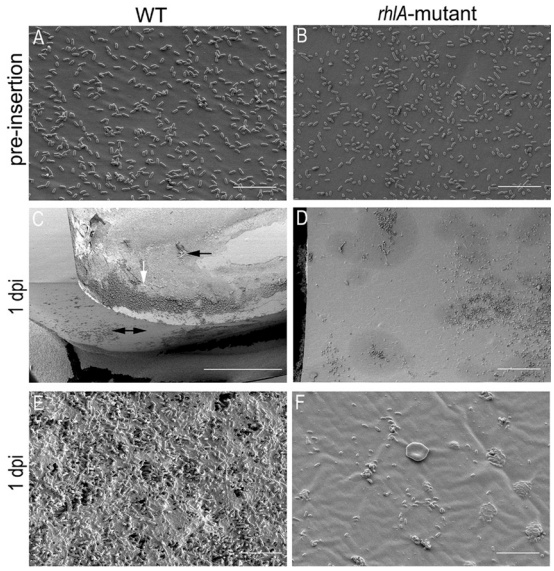

FIG 2 SEM images of biofilm development *in vivo*. (A and B) Images of implants coated with WT *P. aeruginosa* (A) and the *rhlA* mutant (B) pre-insertion. Bars, 10 μm. (C) WT *P. aeruginosa* biofilm being invaded by PMNs at the edge of the implant (white arrow) at 1 dpi. PMNs are also seen on the side of the implant (double-headed black arrow). The single-headed black arrow points to another edge of the biofilm, but mostly the entire interior of the implant was covered with biofilm. Bar, 200 μm. (E) WT biofilm at 1 dpi. Bar, 10 μm. (D and F) Biofilm with the *rhlA* mutant. Bars, 200 μm (D) and 10 μm (F).

which were inserted into the left side of the peritoneal cavity of each mouse (Fig. 1A). When the implants were subsequently removed, they were often encapsulated in fatty tissue, as shown in Fig. 1B.

The bacterial load associated with the implants was measured at 0 h (preinsertion), at 6 h postinsertion (hpi), and at 1 and 2 days postinsertion (dpi) (Fig. 1C). As shown in Fig. 1C, the bacterial load of the *rhlA* mutant was significantly lower than that of the WT at 6 hpi and continued to decrease. These rates of bacterial clearance were similar to our previous data obtained using a flat silicone implant (36).

Biofilm development *in vivo*. Mice received implants precoated with the WT or the *rhlA* mutant or received uncoated implants (sterile implants). At specified time points, the implants were recovered and prepared for SEM and CLSM by being cut in half as shown in Fig. 1A. The distributions of the WT and the *rhlA* mutant on the implants at 0 hpi were uniform in the SEM images (Fig. 2A and B). At 1 dpi, the WT had already formed a biofilm, as shown in Fig. 2C and E. The bacterial load in the biofilm increased visually at 2 and 3 dpi (not shown), but by 7 dpi bacteria were no longer visible and the implants resembled sterile implants (see Fig. S1 in the supplemental material). The *rhlA* mutant did not form a biofilm, and almost no bacteria were visible at 1, 2, 3, or 7 dpi (Fig. 2D and F).

PMN interaction with biofilm *in vivo*. Invasion of PMNs was seen at the edge of the biofilm and is shown in Fig. 2C (white arrow). PMNs were also observed at the side of the implant (double-headed black arrow). The single-headed black arrow in the figure points to another edge of the biofilm, but mostly the entire interior surface of the implants was covered with biofilm. PMNs were observed in contact with the WT strain at 1, 2, and 3 dpi (Fig. 3), progressively becoming embedded in the biofilm matrix. At 2 and 3 dpi, the PMNs all appeared damaged, with cavities in the

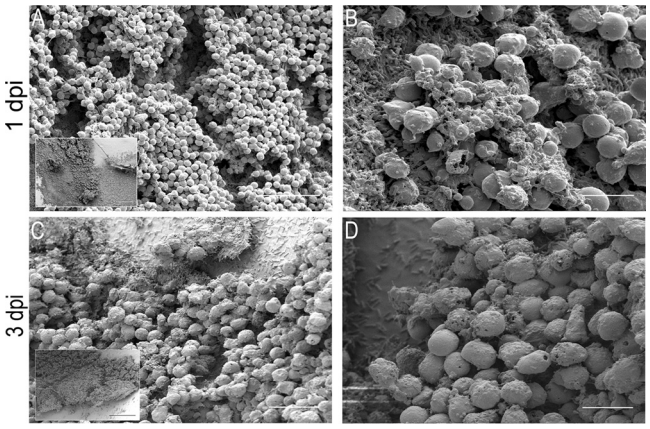

FIG 3 SEM images of WT *P. aeruginosa* biofilm invaded by PMNs. (A and B) Clusters of PMNs on top of the WT *P. aeruginosa* biofilm at 1 dpi. Bars, 50 μm and 10 μm, respectively. In the lower left corner of image A is an image giving an overview of the setting. Bar, 200 μm. (C and D) Images of WT *P. aeruginosa* biofilm at 3 dpi. Bars, 50 μm and 10 μm, respectively. At 3 dpi, the PMNs were imbedded in the biofilm matrix. In the lower left corner of image C is an image giving an overview of the setting. Bar, 200 μm.

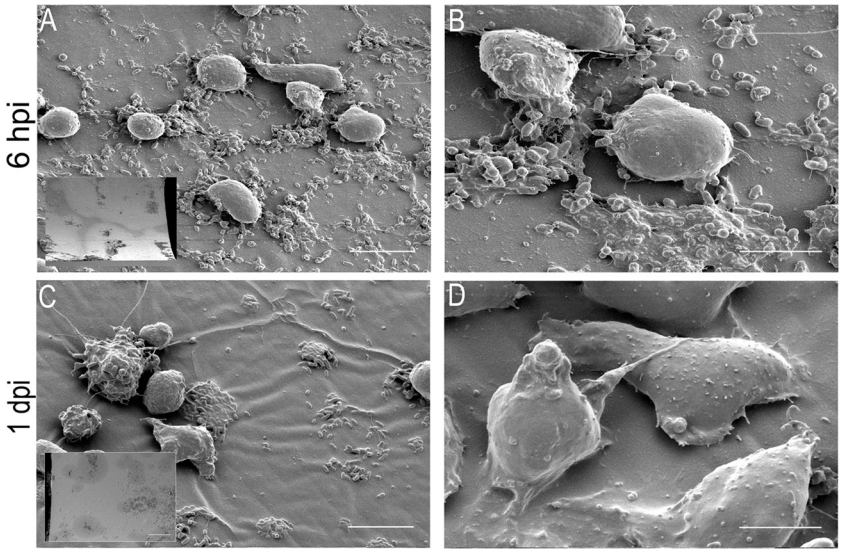

FIG 4 SEM images of *P. aeruginosa rhlA* mutant biofilm and PMNs. The images show implants coated with the *rhlA* mutant at 6 hpi (A and B) and 1 dpi (C and D). Bars, 10 and 5 μm, respectively. The bacteria occurred in clusters, and little biofilm was left by 1 dpi. Panels A and C both contain an image in the lower left corner to give an overview. Bar, 500 μm.

membrane (Fig. 3C and D; see Fig. S2 in the supplemental material). By 6 hpi, numerous PMNs had already been attracted to clear the infection for both strains (Fig. 4A and B; see Fig. 6A). The *rhlA* mutant was cleared rapidly; by 1 dpi, very few bacteria (corresponding to 100-fold fewer CFU than the WT level) but numerous intact PMNs could be seen on the implants (Fig. 4C and D). These results are consistent with the earlier measurements of bacterial load and with our previous observations using the mouse implant model of Christensen et al. (36). The morphologies of the PMNs interacting with the WT and *rhlA* mutant biofilms differed, with a more elongated appearance (indicative of active phagocytosis) for PMNs in contact with the *rhlA* mutant biofilm.

One of the implants with the *rhlA* mutant looked similar to a sterile implant at 1 dpi (see Fig. S3 in the supplemental material), with a thick layer of host cells, including PMNs, encapsulating the implant. We also imaged sterile implants at 1 and 7 dpi, but these implants did not show the same degree of encapsulation by host cells or clustering of actively phagocytosing PMNs as the implants with the *rhlA* mutant (see Fig. S1).

Visualizing the *in vivo* PMN interaction with biofilm by CLSM. Using SEM, we identified PMNs and bacterial biofilms on the implants. To fully confirm that the host cells were PMNs, we used CLSM to visualize the PMN multilobed nucleus, using PI (red) and Syto9 (green) as stains. PI stains the DNA of dead cells or extracellular DNA, and Syto9 stains living cells. The implants were stained directly after removal from the mice and were not fixed. The biofilm and the influx and clustering of PMNs on the implant were easily visualized (Fig. 5A). We observed an increase in dead PMNs on the WT biofilm from 1 to 2 dpi, with all but a few PMNs dead at 2 dpi.

We observed wire-like structures on the implants and speculated that these were extracellular DNA from both bacteria and PMNs. By treating the implants with DNase (Benzonase), we were able to remove the PI-stained strings imaged by CLSM (Fig. 5B). Similar wire-like structures were also observed in the SEM images, in which the structures appear to connect WT bacteria and PMNs (Fig. 6A and 7), but were also seen in SEM images of pure salmon sperm DNA (Fig. 7).

However, SEM investigations of DNase-treated implants revealed that we were not removing all fibers (Fig. 6B and C). We observed a decrease in the matrix material, but the treatment left a vast amount of matrix fibers on the implant. Thus, we cannot conclude that all of the SEM observed wire-like structures were made entirely of DNA, but it was certainly present in the observed matrix.

DISCUSSION

In this study, we developed a foreign body infection model in mice by using hollow silicone tubes to enable visualization of biofilm development, PMN infiltration, and matrix material *in vivo*. The model is an improvement of earlier *in vivo* models, since the hollow tubes prevent peritoneal fluids and blood from covering the area of interest. Thus, only the bacteria and the actively migrating inflammatory cells inside the tubes are exposed for observation when the tubes are opened after being extracted from the mice.

In 2003, Jesaitis et al. (24) used an *in vitro* biofilm model to show paralysis of PMNs on the surface of a *P. aeruginosa* biofilm. The PMNs were rounded and lacked the characteristic polarized morphology of motile, active phagocytosing cells but were still capable of phagocytosing the biofilm below (24). The authors concluded that polarization and migration of PMNs were disrupted by biofilm contact but that the phagocytic and secretory activities were preserved. MacRae et al. (31) made a similar observation in 1980. Using SEM, they observed that human PMNs full of phagocytosed bacteria adopted a smooth rounded surface contour, which they proposed was due to the disappearance of lamellipodia and cell processes. We observed rounded PMN morphology in the SEM images; however, we speculate that the PMNs were dead, since many of them appeared damaged, with obvious cavities in the membrane, after contact with the WT biofilm. Jesaitis et al. (24) also found that areas devoid of biofilm contained actively phagocytic PMNs with a morphology resembling that of implants

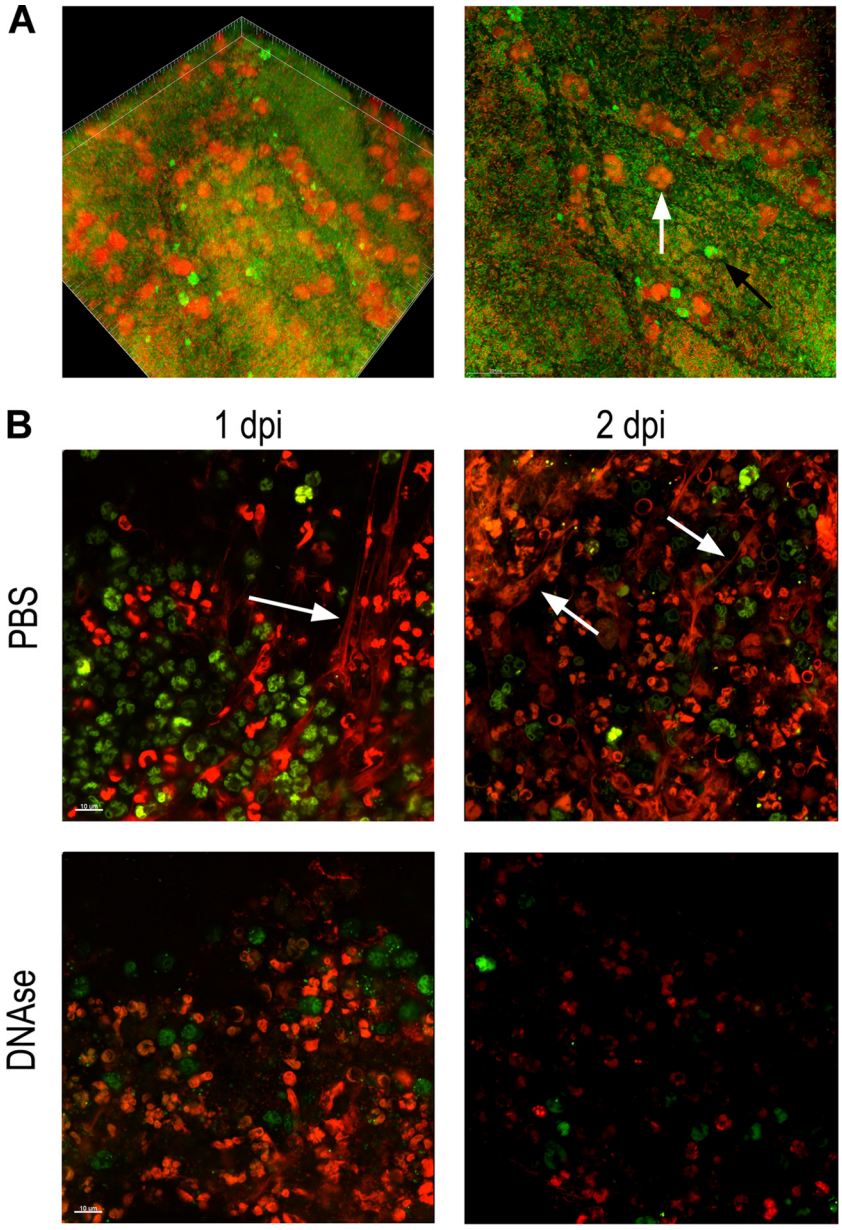

FIG 5 PMNs and wire-like DNA structures on implants visualized with CLSM. Due to the penetration of PI into the cell via the damaged cell membrane, dead cells can be visualized as red fluorescence. The green fluorescence of Syto9 is used to visualized living cells. (A) PMNs on an implant coated with WT *P. aeruginosa* at 1 dpi, stained with PI and Syto9 immediately after removal. Both dead (red) PMNs (white arrow) and some live (green) PMNs (black arrow) are seen. (B) Implants coated with WT *P. aeruginosa* either treated with DNase or not treated (PBS). Wire-like structures on implants not exposed to DNase treatment were imaged at both 1 and 2 dpi (white arrows). On implants treated with DNase, no wire-like structures were imaged.

infected with the *rhlA* mutant or that of sterile implants. Similarly, we previously found that in PMNs exposed to flow chamber biofilms, only those in direct contact with the WT biofilm had impaired phagocytosis and rhamnolipid-mediated lysis (7, 36). The SEM images in the present study clearly indicated that the WT biofilm, but not the *rhlA* mutant biofilm, enabled destruction of the PMNs, thus confirming rhamnolipids as a major *P. aeruginosa* virulence factor. The *in vivo* activity of rhamnolipids has previously been shown in pulmonary infection models, in which an *rhlA* mutant is cleared faster than the WT due to the absence of rhamnolipid-mediated killing of the incoming PMNs (1, 36). The involvement of rhamnolipids has previously been reported for the pathogenesis of CF and the development of ventilator-associated pneumonia (27, 28). In addition to implants, the interaction that we identified between biofilm and PMNs may also be important in the CF lung and in chronic wounds, where PMNs are unable to clear the infection (8, 35).

Bacterial extracellular DNA (eDNA) has been associated with the matrix of the biofilm phenotype, where it is proposed to be a component stabilizing the biofilm structure (40). Allesen-Holm et al. (3) reported that in *P. aeruginosa* biofilms grown in flow cells, eDNA is generated by lysis of a subpopulation of bacteria. How-

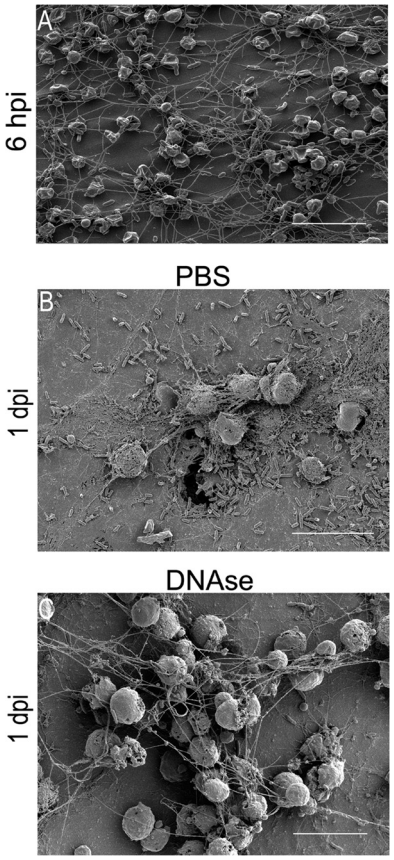

FIG 6 Wire-like structures imaged with SEM. (A) SEM image of an implant with WT *P. aeruginosa* at 6 hpi. Bar, 10 μm. (B) SEM image of a nontreated implant (PBS) at 1 dpi. Bar, 10 μm. (C) SEM image of an implant coated with WT *P. aeruginosa* and treated with DNase at 1 dpi. DNase treatment did not remove the wire-like structures entirely but seemed to reduce the thickness. Bar, 10 μm.

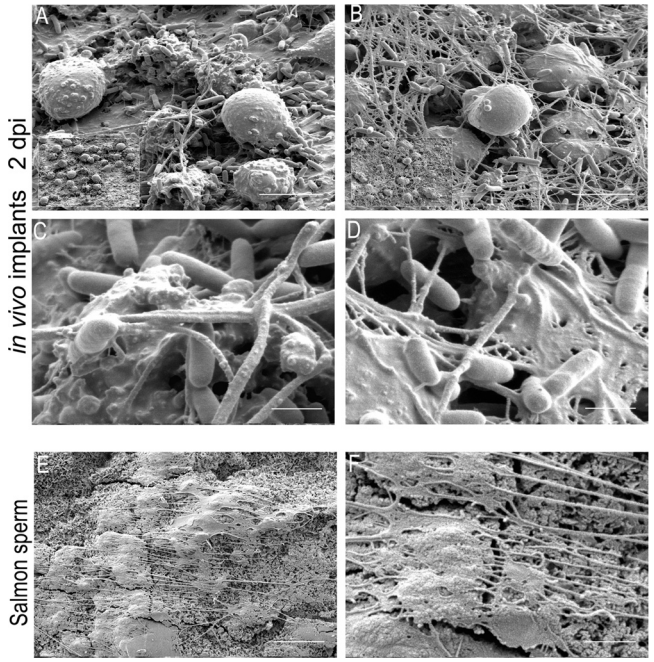

FIG 7 SEM images of wire-like structures on an implant with a WT *P. aeruginosa* biofilm at 2 dpi and on fixated pure salmon sperm DNA, as a control. (A and C) Single area with wire-like structures. (B and D) Net of wire-like structures. (E and F) Wire-like structures very similar to those observed on the implants with a WT *P. aeruginosa* biofilm and PMNs (A to D). Bars, 5 μm (A, B, and E) and 1 μm (C, D, and F). Images A and B both contain an overview of the implant in the lower left corner. Bars, 10 μm.

ever, when the bacteria interacting with host PMNs release rhamnolipids, the PMNs undergo lysis and release their cellular contents, including DNA (23). This release of DNA and actin can also enhance biofilm development (38). Moreover, PMNs can release DNA when they form neutrophil extracellular traps (NETs), which are composed primarily of chromatin DNA, histones, and granule proteins, to kill bacteria (11). Most reported studies of NETs used purified PMNs from human blood, which were activated and studied *in vitro*. Several studies have identified NETs *in vivo*, but by use of histological methods (5, 11, 12). Ermert et al. (20) isolated PMNs from mice but stimulated them *in vitro* for the investigation of NETs. Our study is the first to show the generation of wire-like DNA structures *in vivo*, using unfixed samples and visualization by CLSM and DNA staining. Treatment with DNase indicated that the wire-like structures stained with PI were formed of DNA, since it was possible to locate the wire-like structures only on nontreated implants. The wire-like structures were present only on implants coated with the WT, not on those coated with the *rhlA* mutant, indicating that the structures arise from lysis of PMNs.

The wire-like structures observed with CLSM resemble the wires seen in the SEM images. We speculated that these wires contained DNA and were not artifacts introduced during the preparation for SEM, since pure salmon sperm DNA revealed the same structure. However, treatment with DNase seemed to reduce the thickness of the wires but did not remove them, as seen by CLSM, similar to findings by Alhede et al. (2). Krautgartner et al. (29) showed that fibrin and NETs cannot be discriminated by SEM based on morphological criteria but that CLSM can be used to visualize fully hydrated bacterial biofilms (30), and thereby DNA wires. The origin of the DNA was not determined, and further studies are required to determine whether it arises from bacteria or PMNs.

Using this model, we were able to achieve a high bacterial load on the implants, and visualization of the biofilm developing on the implants confirmed the quantitative bacteriology results we normally see in this mouse model during a 3-day experiment (14a).

In conclusion, we believe that this model provides innovative insight into the unresolved immunological failure of the host defense in clearing chronic biofilm infections. In particular, the underlying mechanisms for the resistance of biofilms to antibiotics and the host immune response, especially PMNs, have not been identified fully. Using this model, we showed that biofilm development *in vivo* depends on the production of virulence factors such as rhamnolipids. Our results emphasize the importance of treating, and perhaps preventing, biofilm infections with agents that target the virulence of biofilm-forming bacteria. In summary, we showed that PMNs are the main immune component in this *in vivo* biofilm model and that they can be destroyed by rhamnolipids produced by WT *P. aeruginosa*. In addition, we showed the presence in the biofilm of eDNA from either bacteria or PMNs, and further studies are required to identify its role in biofilm infections.

ACKNOWLEDGMENTS

We thank Mary-Ann Gleie for preparing the specimens for SEM.

We acknowledge grants to M.G. from the Strategic Research Council and the Villum Foundation.

We declare that we have no competing financial interests.

REFERENCES

1. **Alhede M, et al.** 2009. Pseudomonas aeruginosa recognizes and responds aggressively to the presence of polymorphonuclear leukocytes. Microbiology **155**:3500–3508.
2. **Alhede M, et al.** 2011. Phenotypes of non-attached *Pseudomonas aeruginosa* aggregates resemble surface attached biofilm. PLoS One **6**:e27943. doi:10.1371/journal.pone.0027943.
3. **Allesen-Holm M, et al.** 2006. A characterization of DNA release in *Pseudomonas aeruginosa* cultures and biofilms. Mol. Microbiol. **59**:1114–1128.
4. **Arciola CR, An YH, Campoccia D, Donati ME, Montanaro L.** 2005. Etiology of implant orthopedic infections: a survey on 1027 clinical isolates. Int. J. Artif. Organs **28**:1091–1100.
5. **Beiter K, et al.** 2006. An endonuclease allows Streptococcus pneumoniae to escape from neutrophil extracellular traps. Curr. Biol. **16**:401–407.
6. **Bjarnsholt T, et al.** 2005. Garlic blocks quorum sensing and promotes rapid clearing of pulmonary *Pseudomonas aeruginosa* infections. Microbiology **151**:3873–3880.
7. **Bjarnsholt T, et al.** 2005. *Pseudomonas aeruginosa* tolerance to tobramycin, hydrogen peroxide and polymorphonuclear leukocytes is quorum-sensing dependent. Microbiology **151**:373–383.
8. **Bjarnsholt T, et al.** 2009. *Pseudomonas aeruginosa* biofilms in the respiratory tract of cystic fibrosis patients. Pediatr. Pulmonol. **44**:547–558.
9. **Bjarnsholt T, et al.** 2010. In vitro screens for quorum sensing inhibitors and in vivo confirmation of their effect. Nat. Protoc. **5**:282–293.
10. **Borregaard N.** 2010. Neutrophils, from marrow to microbes. Immunity **33**:657–670.
11. **Brinkmann V, et al.** 2004. Neutrophil extracellular traps kill bacteria. Science **303**:1532–1535.
12. **Buchanan JT, et al.** 2006. DNase expression allows the pathogen group A Streptococcus to escape killing in neutrophil extracellular traps. Curr. Biol. **16**:396–400.
13. **Buret A, Ward KH, Olson ME, Costerton JW.** 1991. An in vivo model to study the pathobiology of infectious biofilms on biomaterial surfaces. J. Biomed. Mater. Res. **25**:865–874.
14. **Christensen LD, et al.** 2007. Impact of *Pseudomonas aeruginosa* quorum sensing on biofilm persistence in an in vivo intraperitoneal foreign-body infection model. Microbiology **153**:2312–2320.

14a. **Christensen LD, et al.** 2012. Synergistic antibacterial efficacy of early combination treatment with tobramycin and quorum-sensing inhibitors against *Pseudomonas aeruginosa* in an intraperitoneal foreign-body infection mouse model. J. Antimicrob. Chemother. **67**:1198–1206.

15. **Costerton JW.** 1999. Introduction to biofilm. Int. J. Antimicrob. Agents **11**:217–221.

15a. **Council of Europe.** 2 December 2005 (amended). European convention for the protection of vertebrate animals used for experimental and other scientific purposes. Strasbourg, France. http://conventions.coe.int/Treaty/en/Treaties/html/123.htm.

16. **Cox G, Crossley J, Xing Z.** 1995. Macrophage engulfment of apoptotic neutrophils contributes to the resolution of acute pulmonary inflammation in vivo. Am. J. Respir. Cell Mol. Biol. **12**:232–237.
17. **Dasgupta MK.** 2002. Biofilms and infection in dialysis patients. Semin. Dial. **15**:338–346.
18. **Davies DG, et al.** 1998. The involvement of cell-to-cell signals in the development of a bacterial biofilm. Science **280**:295–298.
19. **Dougherty SH.** 1988. Pathobiology of infection in prosthetic devices. Rev. Infect. Dis. **10**:1102–1117.
20. **Ermert D, et al.** 2009. Mouse neutrophil extracellular traps in microbial infections. J. Innate Immun. **1**:181–193.
21. **Gjødsbøl K, et al.** 2006. Multiple bacterial species reside in chronic wounds: a longitudinal study. Int. Wound J. **3**:225–231.
22. **Høiby N.** 1974. *Pseudomonas aeruginosa* infection in cystic fibrosis. Relationship between mucoid strains of *Pseudomonas aeruginosa* and the humoral immune response. Acta Pathol. Microbiol. Scand. B Microbiol. Immunol. **82**:551–558.
23. **Jensen PØ, et al.** 2007. Rapid necrotic killing of polymorphonuclear leukocytes is caused by quorum-sensing-controlled production of rhamnolipid by *Pseudomonas aeruginosa*. Microbiology **153**:1329–1338.
24. **Jesaitis AJ, et al.** 2003. Compromised host defense on *Pseudomonas aeruginosa* biofilms: characterization of neutrophil and biofilm interactions. J. Immunol. **171**:4329–4339.
25. **Kirketerp-Møller K.** 2008. Distribution, organization, and ecology of bacteria in chronic wounds. J. Clin. Microbiol. **46**:2717–2722.
26. **Koch B, Jensen LE, Nybroe O.** 2001. A panel of Tn7-based vectors for insertion of the *gfp* marker gene or for delivery of cloned DNA into Gram-negative bacteria at a neutral chromosomal site. J. Microbiol. Methods **45**:187–195.
27. **Kohler T, Guanella R, Carlet J, van Delden C.** 2010. Quorum sensing-dependent virulence during Pseudomonas aeruginosa colonisation and pneumonia in mechanically ventilated patients. Thorax **65**:703–710.
28. **Kownatzki R, Tümmler B, Döring G.** 1987. Rhamnolipid of *Pseudomonas aeruginosa* in sputum of cystic fibrosis patients. Lancet **i**:1026–1027.
29. **Krautgartner WD, et al.** 2010. Fibrin mimics neutrophil extracellular traps in SEM. Ultrastruct. Pathol. **34**:226–231.
30. **Kumoh H.** 1996. Pathogenesis and management of bacterial biofilms in the urinary tract. J. Infect. Chemother. **2**:18–28.
31. **MacRae EK, Pryzwansky KE, Cooney MH, Spitznagel JK.** 1980. Scanning electron microscopic observations of early stages of phagocytosis of E. coli by human neutrophils. Cell Tissue Res. **209**:65–70.
32. **Pamp SJ, Tolker-Nielsen T.** 2007. Multiple roles of biosurfactants in structural biofilm development by *Pseudomonas aeruginosa*. J. Bacteriol. **189**:2531–2539.
33. **Segal AW.** 2005. How neutrophils kill microbes. Annu. Rev. Immunol. **23**:197–223.
34. **Singh PK, et al.** 2000. Quorum-sensing signals indicate that cystic fibrosis lungs are infected with bacterial biofilms. Nature **407**:762–764.
35. **Thomsen TR, et al.** 2010. The bacteriology of chronic venous leg ulcer examined by culture-independent molecular methods. Wound Repair Regen. **18**:38–49.
36. **van Gennip M, et al.** 2009. Inactivation of the *rhlA* gene in *Pseudomonas aeruginosa* prevents rhamnolipid production, disabling the protection against polymorphonuclear leukocytes. APMIS **117**:537–546.
37. **von Eiff C, Jansen B, Kohnen W, Becker K.** 2005. Infections associated with medical devices: pathogenesis, management and prophylaxis. Drugs **65**:179–214.
38. **Walker TS, et al.** 2005. Enhanced Pseudomonas aeruginosa biofilm development mediated by human neutrophils. Infect. Immun. **73**:3693–3701.
39. **Ward KH, Olson ME, Lam K, Costerton JW.** 1992. Mechanism of persistent infection associated with peritoneal implants. J. Med. Microbiol. **36**:406–413.
40. **Whitchurch CB, Tolker-Nielsen T, Ragas PC, Mattick JS.** 2002. Extracellular DNA required for bacterial biofilm formation. Science **295**:1487.